Determination of the $E2/M1$ ratio in the $\gamma N \rightarrow \Delta(1232)$ transition from a simultaneous measurement of $p(\vec{\gamma},p)\pi^0$ and $p(\vec{\gamma},\pi^+)n$

R. Beck,[1] H. P. Krahn,[1] J. Ahrens,[1] J. R. M. Annand,[5] H. J. Arends,[1] G. Audit,[2] A. Braghieri,[3] N. d'Hose,[2] D. Drechsel,[1] O. Hanstein,[1] J. C. McGeorge,[5] R. O. Owens,[5] P. Pedroni,[3] T. Pinelli,[3,4] G. Tamas,[2] L. Tiator,[1] and Th. Walcher[1]

[1]*Institut für Kernphysik, Universität Mainz, 55099 Mainz, Germany*

[2]*Service de Physique Nucléaire-DAPNIA, CEA-Saclay, 91191 Gif-sur-Yvette, France*

[3]*Istituto Nazionale di Fisica Nucleare, Sezione di Pavia, 27100 Pavia, Italy*

[4]*Dipartimento di Fisica Nucleare e Teorica, Università di Pavia, 27100 Pavia, Italy*

[5]*Department of Physics and Astronomy, Glasgow University, Glasgow G12 8QQ, United Kingdom*

(Received 20 April 1999; published 16 February 2000)

Tagged linearly polarized photons have been used at the Mainz Microtron (MAMI) for simultaneous measurements of the $p(\vec{\gamma},p)\pi^0$ and $p(\vec{\gamma},\pi^+)n$ reaction channels to study the $\gamma N \rightarrow \Delta(1232)$ transition. The energy dependence of the magnetic dipole $M_{1+}^{3/2}$ and electric quadrupole $E_{1+}^{3/2}$ amplitudes have been extracted from these data in the photon energy range from 270 to 420 MeV. The $E2/M1$ ratio for the $\gamma N \rightarrow \Delta(1232)$ transition has been determined to be $-(2.5 \pm 0.1_{stat} \pm 0.2_{sys})\%$ at the resonance position ($\delta_{33}=90°$).

PACS number(s): 13.60.Le, 14.20.Gk, 13.60.Rj

I. INTRODUCTION

Low energy electromagnetic properties of baryons, such as mass, charge radius, magnetic and quadrupole moments are important observables for any model of the nucleon structure. In various constituent-quark models a tensor force, in the interquark hyperfine interaction, introduced first by de Rujula, Georgi, and Glashow [1], leads to a d-state admixture in the baryon ground-state wave function. As a result the tensor force induces a small violation of the Becchi-Morpurgo selection rule [2], that the $\gamma N \rightarrow \Delta(1232)$ excitation is a pure $M1$ (magnetic dipole) transition, by introducing a nonvanishing $E2$ (electric quadrupole) amplitude. For chiral quark models or in the Skyrmion picture of the nucleon, the main contribution to the $E2$ strength stems from tensor correlations between the pion cloud and the quark bag or meson exchange currents between the quarks. To observe a static deformation (d-state admixture) a target with a spin of at least 3/2 (e.g., Δ matter) would be required. The only realistic alternative is to measure the transition $E2$ moment in the $\gamma N \rightarrow \Delta$ transition at resonance or, equivalently, the $E_{1+}^{3/2}$ partial wave amplitude in the $\Delta \rightarrow N\pi$ decay. The amplitudes in the $N\pi$ final state are usually denoted by $E_{l\pm}^{I}$ and $M_{l\pm}^{I}$, where E and M are the electric and magnetic multipoles, I is the isospin and l is the orbital angular momentum of the $N\pi$ system, and the $\pm$ sign refers to its total angular momentum $J=l\pm 1/2$.

The experimental quantity of interest compared with the different nucleon models is the ratio $R_{EM}=E2/M1=E_{1+}^{3/2}/M_{1+}^{3/2}$ of the electric quadrupole $E2$ to the magnetic dipole $M1$ amplitude in the region of the $\Delta(1232)$ resonance. In quark models with $SU(6)$ symmetry, for example, the MIT bag model, $R_{EM}=0$, is predicted. Depending on the size of the hyperfine interaction and the bag radius, broken $SU(6)$ symmetry leads to $-2\% < R_{EM} < 0$ [3–6]. Larger negative values in the range $-6\% < R_{EM} < -2.5\%$ have been predicted by Skyrme models [7], while results from chiral bag models [8] give values in the range -2 – -3%. The first Lattice QCD result is $R_{EM}=(+3\pm 9)\%$ [9] and a quark model with exchange currents yields values of about -3.5% [10].

The determination of the quadrupole strength $E2$ in the region of the $\Delta(1232)$ resonance has been the aim of a considerable number of experiments and theoretical activities in the last few years. Very recently, new experimental results have been published for the differential cross section and photon asymmetry of pion photoproduction off the proton from the Mainz Microtron (MAMI) and the laser backscattering facility (LEGS) at Brookhaven National Laboratory, with the results $R_{EM}=-(2.5\pm 0.2_{stat}\pm 0.2_{sys})\%$ from the Mainz group [11] and $R_{EM}=-(3.0\pm 0.3_{stat+sys} \pm 0.2_{mod})\%$ from the LEGS group [12]. These new R_{EM} results have started intense discussions about the correct way to extract the $E2/M1$ ratio from the new experimental data. In particular, the large variation in the R_{EM} values obtained in theoretical analyses of these data at RPI [13] ($R_{EM}=-(3.2\pm 0.25)\%$), VPI [14] ($R_{EM}=-(1.5\pm 0.5)\%$), and Mainz [15] ($R_{EM}=-(2.5\pm 0.1)\%$) was quite unsatisfactory.

In this paper we present the MAMI $p(\vec{\gamma},p)\pi^0$ and $p(\vec{\gamma},\pi^+)n$ differential cross sections and photon asymmetries, and discuss in detail different analyses to extract the s- and p- partial wave amplitudes and the $E2/M1$ ratio. In Sec. II we briefly describe the experimental setup and show a selection of the measured cross sections and photon asymmetries for both pion production channels from the proton in Sec. III. The essential ingredients of a multipole analysis are outlined in Sec. IV. Three different analyses of our data to extract the s- and p-partial wave amplitudes and the $E2/M1$ ratio are discussed in Secs. V and VI. We conclude with a summary and outlook in Sec. VII.

II. EXPERIMENTAL SETUP AND DATA ANALYSIS

Since the experimental setup used for this measurement was described in detail in Ref. [16], we will restrict the present discussion to the main features of the experiment.

Linearly polarized photons were produced by coherent bremsstrahlung in a 100-μm-thick diamond crystal [17,18]. The photon energy was determined by the Glasgow tagging spectrometer at the Mainz Microtron (MAMI) [19] which, in a 352-channel focal plane detector, analyzes the momentum of the electron that has radiated the bremsstrahlung photon [20]. This detector system is able to energy tag photons in the range of 50–800 MeV with a resolution of about 2 MeV [21]. The collimation of the photon beam yielded a tagging efficiency of about 55% for incoherent bremsstrahlung. To continuously monitor the tagging efficiency and the photon polarization, a pair detector was used downstream of the hadron detector DAPHNE. This pair detector consists of a 0.5-mm-thick Cu converter followed by two 2-mm-thick plastic scintillators operated in coincidence. Its efficiency ($\epsilon \simeq 3\%$ for photons) was regularly checked with a lead glass detector ($\epsilon \simeq 100\%$ for photons) in calibration runs at low beam intensity. The photon polarization was determined from the photon spectrum measured by the tagging spectrometer in coincidence with the pair detector and with the aid of theoretical calculations [22]. The quality of these calculations was tested by an absolute measurement of the photon polarization using coherent π^0 photoproduction on ^{4}He as a polarimeter reaction with an analyzing power $A=100\%$. Excellent agreement between calculations and experiment was found [23] and, in this way, both the photon polarization and the photon flux could be determined with an absolute precision of better than $\pm 2\%$.

The liquid hydrogen cryogenic target was contained in a 43-mm-diameter, 275-mm-long Mylar cylinder with a wall thickness of 0.1 mm. The target density was stabilized and determined to an accuracy of $\pm 0.5\%$ by means of an automatic pressure and temperature control system.

The reaction products, the recoil proton from $\gamma p \rightarrow p \pi^0$ and the pion from $\gamma p \rightarrow n \pi^+$ were detected using the large acceptance detector DAPHNE ($21° \leqslant \theta \leqslant 159°$, $0° \leqslant \phi \leqslant 360°$) built by the CEA/DAPNIA-SPhN at Saclay and the INFN sezione di Pavia [24]. Good definition of the charged particle tracks was obtained from the central vertex detector consisting of three coaxial cylindrical multiwire proportional chambers providing a polar angular resolution of $\Delta\theta \leqslant 1°$ full width at half maximum (FWHM) and an azimuthal resolution $\Delta\phi \leqslant 2°$ FWHM. This vertex detector is surrounded by a segmented $\Delta E - E - \Delta E$ plastic scintillator telescope with successive thicknesses of 10 mm, 100 mm, and 5 mm, respectively. The outermost layer is a lead-aluminum scintillator sandwich designed to enhance the π^0 detection efficiency and to provide additional energy loss information for charged particles.

In the first step of the analysis those events were selected, that had only one charged trajectory with its polar angle in the range $21° \leqslant \theta \leqslant 159°$. After this cut, the basic task of the data analysis was to identify the pions and protons. This separation was performed by using a range method as described in detail in Ref. [25], which simultaneously uses all of the measured energy losses in the scintillator layers of DAPHNE to identify charged hadrons (π^+, p) and to determine their energy. A restriction made on the vertex position, defined as the point on the reconstructed track, which lies closest to the detector axis, ensured a complete rejection of particles coming from the target windows and walls. As a result no empty target subtraction was needed.

The main contributions to the systematic error in the determination of the unpolarized differential cross section are due to uncertainties in the photon flux ($\pm 2\%$), the target density ($\pm 0.5\%$), and ($\pm 2\%$) for the proton/pion separation with the range method.

III. EXPERIMENTAL RESULTS

In single pion photoproduction, the differential cross section for linearly polarized photons and unpolarized targets is given by the expression

$$\frac{d\sigma(\theta,\phi)}{d\Omega} = \frac{d\sigma_0(\theta)}{d\Omega}[1 - \Sigma(\theta)\cos(2\phi)], \qquad (1)$$

where Σ is the photon asymmetry, and θ and ϕ are the polar and azimuthal angles of the pion with respect to the beam direction. Since DAPHNE has full 2π azimuthal coverage it allows a direct measurement of the ϕ dependence of the differential cross section and, therefore, the determination of Σ and the unpolarized cross section $d\sigma_0/d\Omega$ at the same time.

A selection of the measured cross sections and photon asymmetries in the c.m. frame for the $\gamma p \rightarrow p \pi^0$ and $\gamma p \rightarrow n \pi^+$ reaction channels [11,26] are shown in Figs. 1–4. This is the first data set for which the two observables $d\sigma_0/d\Omega$ and Σ have been measured simultaneously at all angles and photon energies for both pion production channels from the proton. The measurement covers the whole $\Delta(1232)$ resonance region in 16 energy bins between $E_\gamma = 270$ and 420 MeV, where E_γ is the tagged photon energy in the lab frame. The angular distributions for $d\sigma_0/d\Omega$ and Σ were measured from 45° up to 135° for the $n\pi^+$ channel. In the $p\pi^0$ case the angular range varied from 95° to 125° at $E_\gamma = 270$ MeV to 65° to 125° for the highest energy point at $E_\gamma = 420$ MeV. In Figs. 1–4 the result of a fixed-t dispersion relation analysis [27], which will be discussed below, is shown as a solid line. Our differential cross sections and asymmetries are in good agreement with the dispersion relation analysis except for the differential cross sections around 330 MeV where we find a slight discrepancy.

Figures 5 and 6 compare the energy dependence of the present MAMI results and the recent LEGS results [12] for $\gamma p \rightarrow p \pi^0$ at $\theta_{\pi^0} = 90°$ and $\gamma p \rightarrow n \pi^+$ at $\theta_{\pi^+} = 85°$. For the LEGS results the statistical error and the angle and energy dependent error have been evaluated point by point and combined to the net uncertainty bars, which are shown in Figs. 5 and 6. The error bars on the MAMI points are only statistical. The systematic scale uncertainties are $\sim 3\%$ for the MAMI results and $\sim 1\%$ for the LEGS results. There is an energy dependent discrepancy of up to 15% between the absolute differential cross sections. For both $\gamma p \rightarrow p \pi^0$ and $\gamma p \rightarrow n \pi^+$, the LEGS cross sections start to rise above the MAMI data at $E_\gamma = 280$ MeV, reaching $\simeq 15\%$ higher values at the highest energy LEGS data point at $E_\gamma = 323$ MeV. Since the difference is energy dependent it will

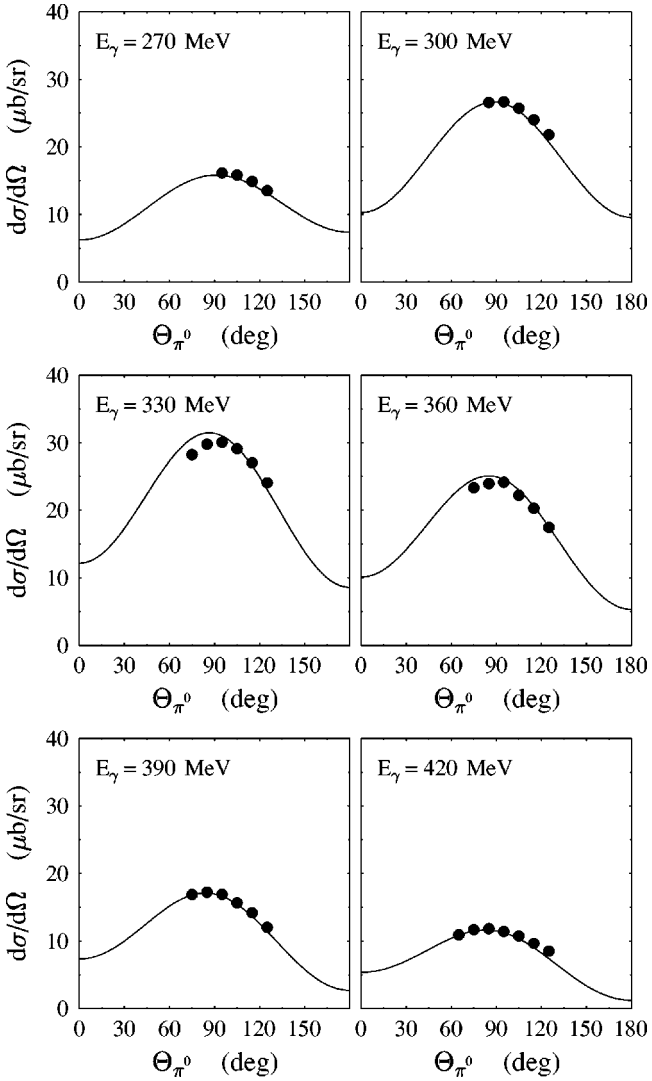

FIG. 1. The differential cross section $d\sigma/d\Omega$ for $p(\gamma,p)\pi^0$ at six different photon energies. The solid line shows the result of the energy dependent multipole analysis.

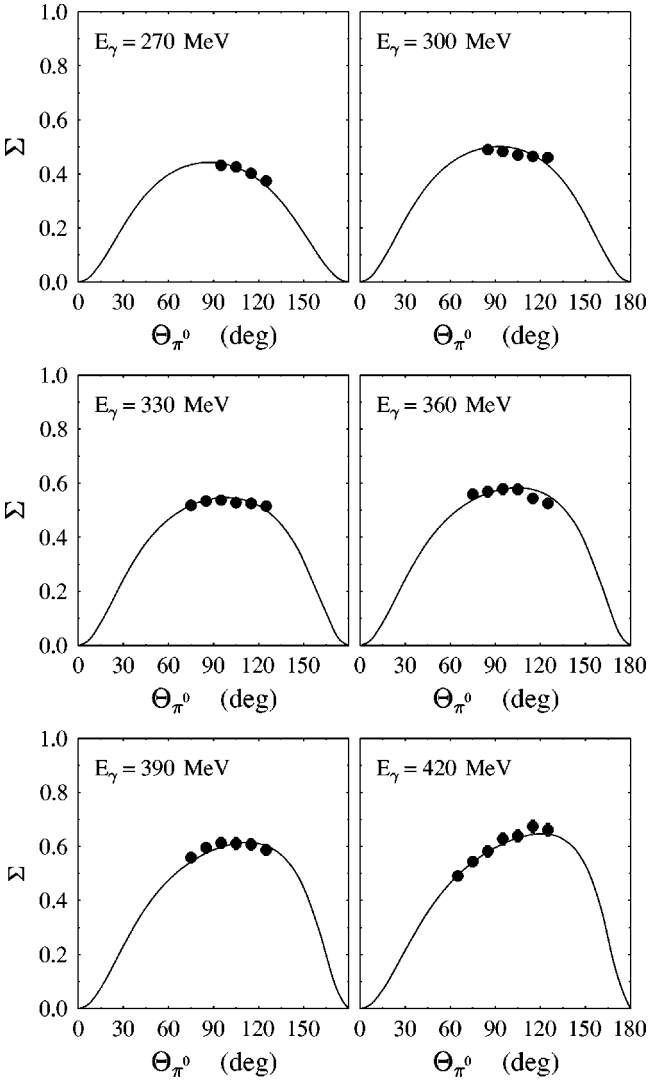

FIG. 2. The photon asymmetry Σ for $p(\vec{\gamma},p)\pi^0$ at six different photon energies. The solid line shows the result of the energy dependent multipole analysis.

affect the absolute values of the resonant partial waves $M_{1+}^{3/2}$ and $E_{1+}^{3/2}$ (see discussion below).

In Fig. 7 the LEGS and MAMI angular distributions for the differential cross section and the photon asymmetry are compared at $E_\gamma = 320$ MeV for $p(\vec{\gamma},p)\pi^0$ and $p(\vec{\gamma},\pi^+)n$. One sees that the differential cross sections differ not only in absolute magnitude, but also in angular shape. The two most forward angular points at $\theta_{\pi^0} = 70°$ and 80° of the LEGS $p\pi^0$ differential cross section drop faster than the MAMI results. The same behavior is seen for the $n\pi^+$ cross section at $\theta_{\pi^+} = 20°$, 150°, and 170°. This difference in the shape of the differential cross sections for the two data sets will play an important role in the discussion of the non-Born contribution for partial waves with $l_\pi \geq 2$. On the other hand, the photon asymmetry agrees well for the $p\pi^0$ channel and shows only small differences for the $n\pi^+$ data, where the MAMI results are slightly above the LEGS data.

IV. MULTIPOLE ANALYSIS OF THE MAMI DATA

A. General aspects

In $\gamma N \to N\pi$ both incident particles and the final nucleon have two spin states yielding in eight degrees of freedom. From parity conservation this is reduced to a total number of four complex amplitudes to describe the reaction. Allowing for one arbitrary phase factor, there are therefore seven independent physical quantities which need to be measured at any setting of E_γ and θ_π. Different sets of amplitudes are used in the literature, e.g., the helicity amplitudes (H_1,H_2,H_3,H_4) introduced by Jacob and Wick [28] or the Pauli amplitudes (F_1,F_2,F_3,F_4) by Chew, Goldberger, Low, and Nambu [29]. While the observables of single pion photoproduction are more elegantly expressed by the helicity amplitudes, the Pauli amplitudes are particularly suited for decomposition into partial waves [30,31].

A complete database for pion photoproduction (the ''complete'' experiment) requires at least eight independent

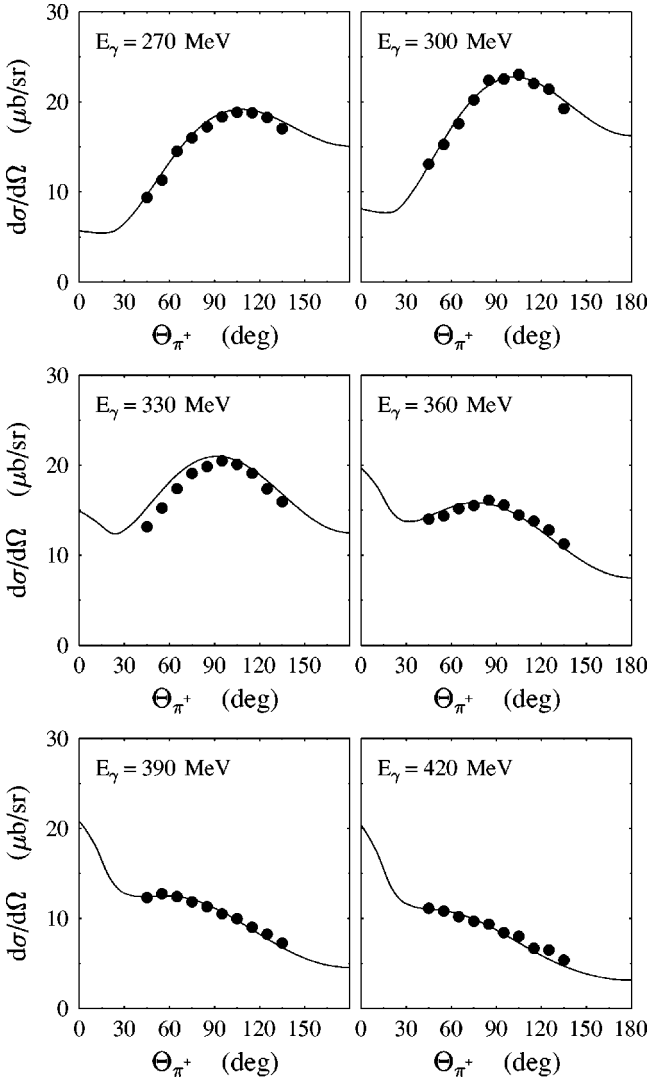

FIG. 3. The differential cross section $d\sigma/d\Omega$ for $p(\gamma,\pi^+)n$ at six different photon energies. The solid line shows the result of the energy dependent multipole analysis.

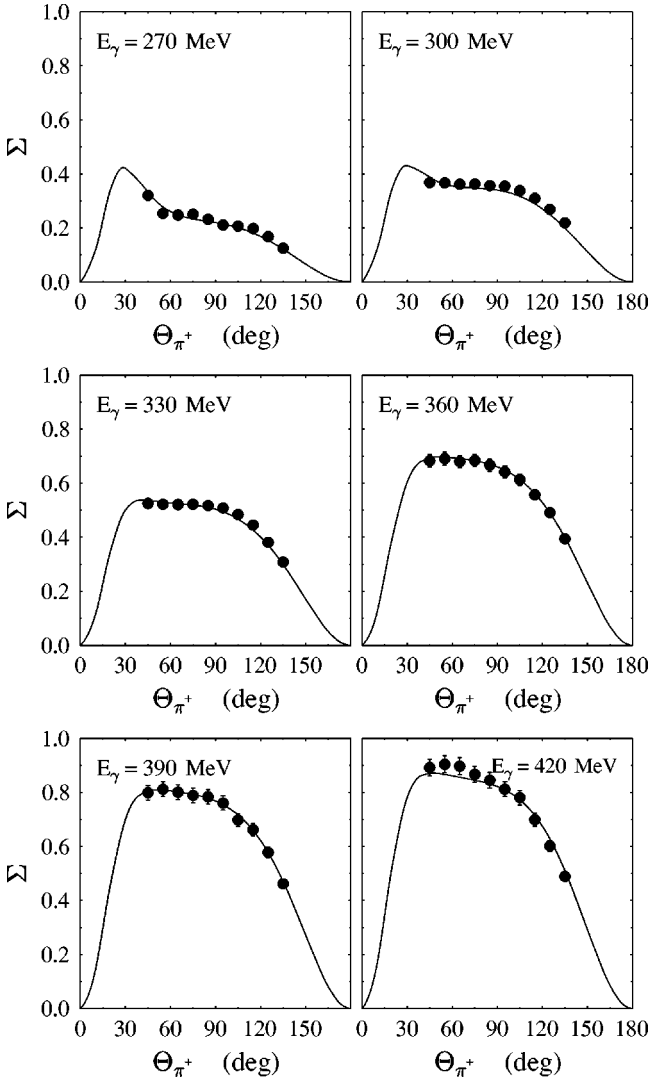

FIG. 4. The photon asymmetry Σ for $p(\vec{\gamma},\pi^+)n$ at six different photon energies. The solid line shows the result of the energy dependent multipole analysis.

observables to specify the multipole amplitudes to all orders in l_π [32–34]. Such complete information is not available at present and standard multipole analyses have to rely on the differential cross section $d\sigma/d\Omega$ and the three single polarization observables Σ (photon asymmetry), P (recoil nucleon polarization), and T (target asymmetry). For pion photoproduction from threshold up to the $\Delta(1232)$ resonance region, these four observables provide sufficient conditions for a complete database, if the higher partial waves $l_\pi \geqslant 2$ can be adequately represented by the Born contributions. This approach is expected to be appropriate up to the region of the higher resonances ($E_\gamma \simeq 600$ MeV) and even they may affect only certain multipoles (e.g., $D_{13}(1520) \leftrightarrow E_{2-}$, M_{2-}). Such arguments were used by Grushin [35] to analyze the Kharkov data [36] ($d\sigma/d\Omega$, Σ, P, and T) for $\gamma p \rightarrow p\pi^0$ and $\gamma p \rightarrow n\pi^+$. In their analysis both the real and imaginary parts of the s and p wave amplitudes could be determined for the first time independently of the pion-nucleon phase shifts $\delta_{IJ}^{\pi N}$. The mean difference between the $\delta_{33}^{\gamma,\pi N}$ phase from the Kharkov analysis and the known pion-nucleon scattering phase $\delta_{33}^{\pi N}$ was only $-(2.3\pm 0.5)°$ over the entire energy range $E_\gamma = 250-500$ MeV.

The $p\pi^0$ and $n\pi^+$ multipole amplitudes $\mathcal{M}_{l\pm}$ ($\mathcal{M}_{l\pm}$ stands for E_{0+}, M_{1-}, ...) are related to the isospin 1/2 and 3/2 components $\mathcal{M}_{l\pm}^{1/2}$ and $\mathcal{M}_{l\pm}^{3/2}$ by

$$\mathcal{M}_{l\pm}(p\pi^0) = \mathcal{M}_{l\pm}^{1/2} + \frac{2}{3}\mathcal{M}_{l\pm}^{3/2}, \tag{2}$$

$$\mathcal{M}_{l\pm}(n\pi^+) = \sqrt{2}\left(\mathcal{M}_{l\pm}^{1/2} - \frac{1}{3}\mathcal{M}_{l\pm}^{3/2}\right). \tag{3}$$

The multipole amplitudes $\mathcal{M}_{l\pm}^{I}$ are complex functions of the c.m. energy W. Below the two-pion production threshold ($E_\gamma \simeq 310$ MeV), the Fermi-Watson theorem [37] allows one to express the phases of the complex multipole amplitudes by the corresponding pion-nucleon scattering phase shifts $\delta_{l\pm}^{I}$

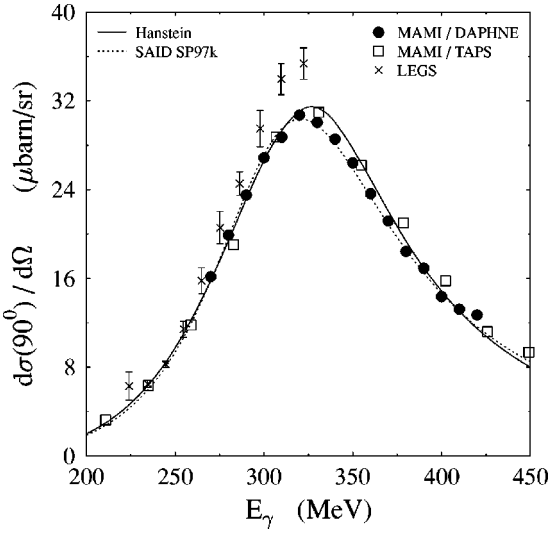

FIG. 5. The energy dependence of the differential cross section at $\theta_{\pi^0}=90°$ for $p(\gamma,p)\pi^0$ in comparison with our energy dependent multipole analysis (full line) and the VPI solution SP97k (dotted line). For the LEGS points the statistical error and part of the systematic error are combined to the net uncertainty bars [61]. The error bars on the MAMI/DAPHNE points [26] and the MAMI/TAPS results [42] are only statistical. The systematic scale uncertainties are ~2% for LEGS, ~4% for MAMI/DAPHNE, and ~6% for MAMI/TAPS.

$$\mathcal{M}^I_{l\pm}=|\mathcal{M}^I_{l\pm}|\exp(i\,\delta^I_{l\pm}+n\pi), \tag{4}$$

where I can be 1/2 and 3/2, and n is an integer. However, even at energies of about 400 MeV, the πN inelasticities in the P_{33} partial wave are very small, which suggests that the Fermi-Watson theorem can be applied well above the two-pion threshold.

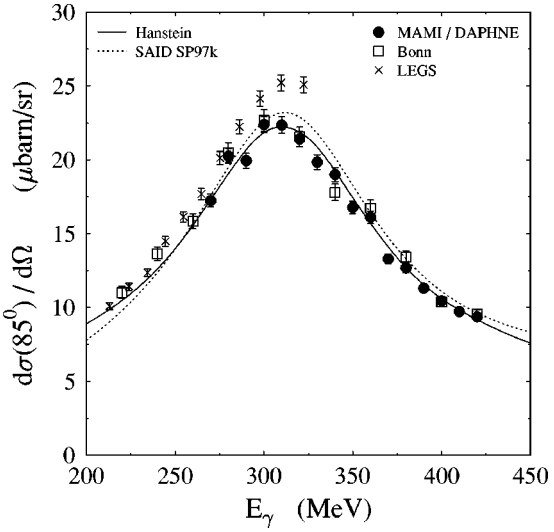

FIG. 6. The energy dependence of the differential cross section at $\theta_{\pi^+}=85°$ for $p(\gamma,\pi^+)n$ in comparison with our energy dependent multipole analysis (full line) and the VPI solution SP97k (dotted line). For the LEGS points the statistical error and part of the systematic error are combined to the net uncertainty bars [61]. The error bars on the MAMI points [26] and the Bonn results [48] are only statistical. The systematic scale uncertainties are ~2% for LEGS, ~4% for MAMI, and ~6% for Bonn.

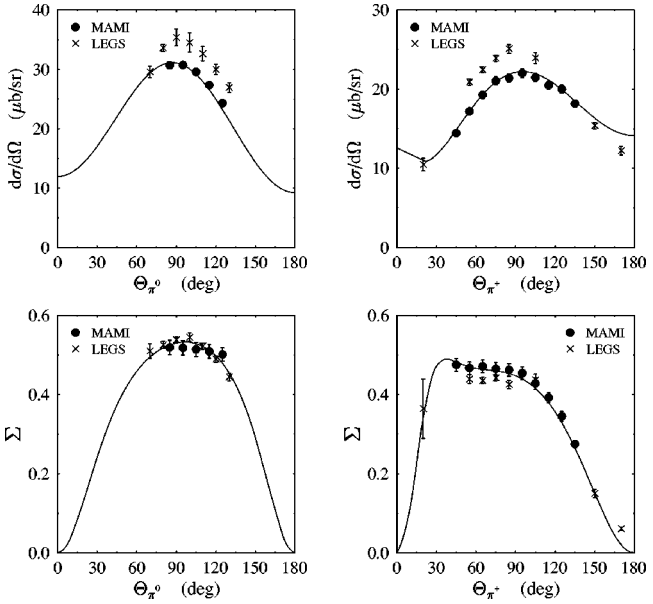

FIG. 7. The differential cross section $d\sigma/d\Omega$ and the photon asymmetry Σ for $p(\vec{\gamma},p)\pi^0$ (left) and $p(\vec{\gamma},\pi^+)n$ (right) at $E_\gamma=320$ MeV. The MAMI data are compared to the results of LEGS and our energy dependent multipole analysis (full line). For the LEGS points the statistical error and part of the systematic error are combined to the net uncertainty bars [61]. The error bars on the MAMI points [26] are only statistical. The systematic scale uncertainties for $d\sigma/d\Omega$ are ~2% for LEGS, ~4% for MAMI, and ~2% for the photon asymmetry of MAMI.

There exist two basic methods to extract the multipole amplitudes from the database: the ''energy independent'' and the ''energy dependent'' approach. In the energy independent approach, each energy is investigated independently by the use of standard χ^2 minimization techniques, the fit parameters being the real and imaginary parts of the multipole amplitudes $\mathcal{M}^I_{l\pm}$. Below the two-pion production threshold the Fermi-Watson theorem is used, which reduces the number of the necessary observables for a complete experiment by a factor of 2, because only the absolute values $|\mathcal{M}^I_{l\pm}|$ of the partial wave amplitudes need to be determined from the fit. In the energy dependent approach, the data at all energies are analyzed simultaneously. Either an energy dependent parametrization of the partial wave amplitudes must be assumed or, as in our case, the energy dependence is taken from dispersion relations. The principal advantage of this method is that continuity is built in from the beginning and systematic errors tend to cancel out. In some cases one or the other of these two approaches is to be preferred. If the data are closely spaced in energy and cover both differential cross sections and polarization observables (''complete experiment'') at each energy, the energy independent approach is more advantageous. If, on the other hand, the data are widely spaced and only few polarization observables are available, the energy dependent approach is the better one. This approach is also useful if the general resonance struc-

ture is already known and the main interest is to obtain the small partial wave amplitudes. However, the experimental data has to cover the complete energy range of the dominating resonances in order to allow a reliable separation. For instance, in the case of the M_{1+} amplitude in the $\gamma N \rightarrow \Delta(1232)$ transition, one has to cover the complete resonance region (250−450 MeV) to get the M_{1+} multipole as precise as possible [38,35].

B. Higher partial waves

A general problem common to both the energy dependent and the energy independent approach is to decide at which value of the angular momentum l_π the partial wave expansion should be truncated in the fit and how to approximate the higher partial waves. The maximum value n_{max} that the data can determine is found by fitting the angular distributions to a Legendre series or, equivalently, a power series expansion in $\cos\theta$:

$$\frac{d\sigma}{d\Omega} = \frac{q}{k} \sum_{n=0}^{n_{max}} A^n \cos^n \theta, \tag{5}$$

$$\Sigma \frac{d\sigma}{d\Omega} \frac{1}{\sin^2 \theta} = \frac{q}{k} \sum_{n=0}^{n_{max}} A_\Sigma^n \cos^n \theta, \tag{6}$$

$$T \frac{d\sigma}{d\Omega} \frac{1}{\sin \theta} = \frac{q}{k} \sum_{n=0}^{n_{max}} A_T^n \cos^n \theta, \tag{7}$$

$$P \frac{d\sigma}{d\Omega} \frac{1}{\sin \theta} = \frac{q}{k} \sum_{n=0}^{n_{max}} A_P^n \cos^n \theta. \tag{8}$$

The experimentally accessible polynomial coefficients A^n are quadratic or bilinear products of the electric $E_{l\pm}$ and magnetic $M_{l\pm}$ multipole amplitudes.

In this section we examine the sensitivity to higher partial wave contributions of the coefficients A^n and A_Σ^n extracted from the present data. The difference of the cross sections for the photon polarization perpendicular and parallel to the reaction plane, $d\sigma_\perp/d\Omega - d\sigma_\parallel/d\Omega$, is particularly sensitive to higher partial waves. With partial waves up to $l_\pi = 2$, the difference

$$\frac{1}{2\sin^2\theta}\left(\frac{d\sigma_\perp}{d\Omega} - \frac{d\sigma_\parallel}{d\Omega}\right) = \Sigma \frac{d\sigma}{d\Omega} \frac{1}{\sin^2\theta} = \frac{q}{k}(A_\Sigma + B_\Sigma \cos\theta + C_\Sigma \cos^2\theta) \tag{9}$$

has three polynomial coefficients A_Σ, B_Σ, and C_Σ with

$$A_\Sigma \simeq A_\Sigma(s_{wave}, p_{wave}) + \mathrm{Re}[E_{0+} d^*_{wave}] + |d_{wave}|^2, \tag{10}$$

$$B_\Sigma \simeq \mathrm{Re}[(M_{1+} - M_{1-}) d^*_{wave}], \tag{11}$$

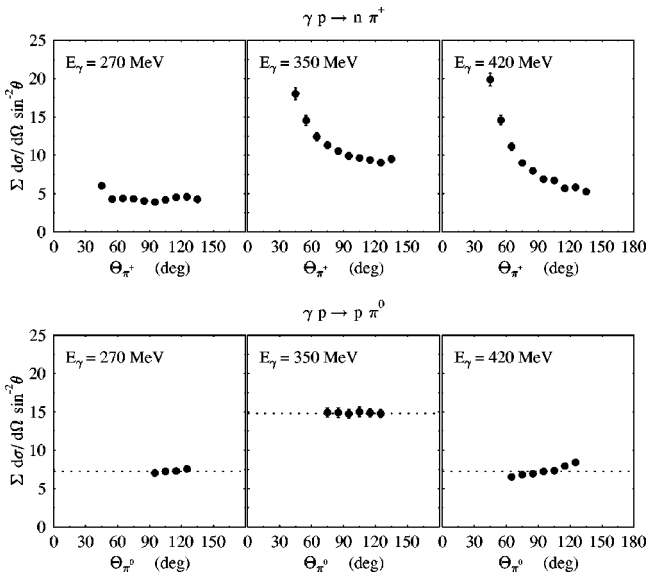

FIG. 8. The difference of the linear polarization cross sections, $(d\sigma_\perp/d\Omega - d\sigma_\parallel/d\Omega)/(2\sin^2(\theta)) = \Sigma d\sigma/d\Omega \sin^{-2}\theta$ for $p(\vec{\gamma}, p)\pi^0$ and $p(\vec{\gamma}, \pi^+)n$.

$$C_\Sigma = |d_{wave}|^2. \tag{12}$$

In the case where only the s wave (E_{0+}) and p waves (M_{1+}, M_{1-}, and E_{1+}) contribute, this difference would be proportional to A_Σ and, therefore, independent of the pion angle θ. The multipole dependence of the coefficients A_Σ, B_Σ, and C_Σ is described in Appendix A.

Figure 8 shows the difference of $d\sigma_\perp/d\Omega - d\sigma_\parallel/d\Omega$ for both pion reaction channels on the proton at our lowest photon energy $E_\gamma = 270$ MeV, at $E_\gamma = 350$ MeV, and at our highest energy $E_\gamma = 420$ MeV. In the $p\pi^0$ channel one recognizes only above the resonance a small deviation from the constant behavior. This is due entirely to the Born contribution to the B_Σ coefficient, i.e., the interference between the real part of the dominant M_{1+} amplitude and the real part of the d-wave amplitudes, for example, in terms like $\mathrm{Re}(M_{1+} - M_{1-})\mathrm{Re}\,E_{2-}$. Such contributions become extremely small at resonance since $\mathrm{Re}(M_{1+} - M_{1-}) \simeq 0$.

The behavior of the difference, $d\sigma_\perp/d\Omega - d\sigma_\parallel/d\Omega$, for the $\vec{\gamma}p \rightarrow p\pi^0$ data from the LEGS collaboration is different. Their observed angular dependence seems to require a sizeable non-Born contribution from d and f waves. The origin of the different angular dependence of the LEGS results for $d\sigma_\perp/d\Omega - d\sigma_\parallel/d\Omega$ arises from the different shape of their unpolarized cross section data. The LEGS photon asymmetries alone are well described by our multipole fit which takes Born contributions in higher partial waves of $l_\pi \geqslant 2$ into account.

In contrast, the difference of $d\sigma_\perp/d\Omega - d\sigma_\parallel/d\Omega$ for $\vec{\gamma}p \rightarrow n\pi^+$ shows a strong angular dependence at all energies. The main reason is that in charged pion photoproduction the pion pole Born graph leads to significant contributions of higher partial waves.

The sensitivity of the differential cross section to higher partial waves is most pronounced at the extreme forward and backward angles. Taking partial waves up to $l_\pi = 2$, the differential cross section is

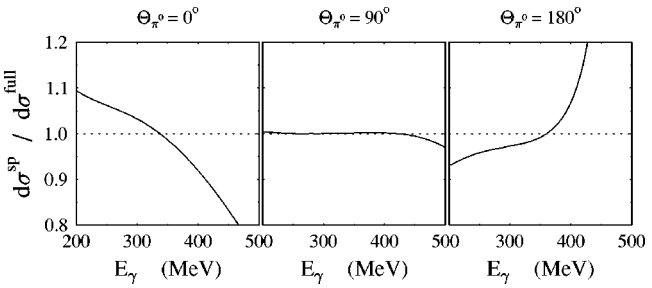

FIG. 9. The contribution of higher partial waves ($l_\pi \geq 2$) to the differential cross section for $\gamma p \to p\pi^0$ at $\theta_\pi = 0°$, $\theta_\pi = 90°$, and $\theta_\pi = 180°$. The solid line is the ratio ($d\sigma^{sp}/d\sigma^{full}$) of the differential cross section for only s and p waves to the differential cross section including higher partial wave contributions (Born contribution for $l_\pi \geq 4$). The curves are obtained from SAID [39] solution SM95.

$$\frac{d\sigma}{d\Omega} = \frac{q}{k}[A + B\cos(\theta) + C\cos^2(\theta) + D\cos^3(\theta) + E\cos^4(\theta)], \quad (13)$$

with five coefficients of the form

$$A \simeq A(s_{wave}, p_{wave}) + \mathrm{Re}[E_{0+} d^*_{wave}] + |d_{wave}|^2, \quad (14)$$

$$B \simeq B(s_{wave}, p_{wave}) + \mathrm{Re}[(M_{1+} - M_{1-}) d^*_{wave}], \quad (15)$$

$$C \simeq C(s_{wave}, p_{wave}) + \mathrm{Re}[E_{0+} d^*_{wave}] + |d_{wave}|^2, \quad (16)$$

$$D \simeq \mathrm{Re}[(M_{1+} - M_{1-}) d^*_{wave}], \quad (17)$$

$$E = |d_{wave}|^2. \quad (18)$$

The effect of the d waves is largest for the coefficients B and D because of an interference term between the large M_{1+} amplitude and the d waves. However, the contributions of these terms can be neglected at the top of the resonance ($\delta_{33} = 90°$). As an example this is illustrated for the combination

$$\mathrm{Re}[(M_{1+} - M_{1-}) E^*_{2-}] = \mathrm{Re}(M_{1+} - M_{1-})\,\mathrm{Re}\,E_{2-} + \mathrm{Im}(M_{1+} - M_{1-})\,\mathrm{Im}\,E_{2-}, \quad (19)$$

where the first term vanishes, because $\mathrm{Re}(M_{1+} - M_{1-})$ passes through zero at the resonance position ($\delta_{33} = 90°$) and the second term can be neglected, because $\mathrm{Im}\,E_{2-}$ is small due to the small d-wave phase. Figure 9 illustrates the sensitivity of the differential cross section to higher partial waves. The solid line shows the ratio ($d\sigma^{sp}/d\sigma^{full}$) of the differential cross section for only s- and p-wave contributions to the differential cross section with higher partial waves. The calculated cross section ratio is shown at the pion angles $\theta_{\pi^0} = 0°$, 90°, and 180° in the energy region between 200 and 500 MeV. For this calculation [39] the SAID solution SM95 was used, in which partial waves up to $l_\pi = 3$ were allowed to vary to fit the data set, but the normal Born contribution was assumed for $l_\pi \geq 4$. At $\theta_{\pi^0} = 90°$, the contributions from the higher partial waves are far below 1%, because they arise only from an interference term with the small s wave E_{0+}, for example, in the form $\mathrm{Re}(E_{0+} d^*_{wave})$ as in Eq. (15). Below and above the $\Delta(1232)$ resonance, however, contributions from $l_\pi \geq 2$ are of the order of 10–20 % of the differential cross section at 0° and 180°. These contributions arise almost completely from the interference between the dominant M_{1+} amplitude and the Born parts of the higher partial waves. In our analysis there are no indications of significant non-Born contributions for higher partial waves ($l_\pi \geq 2$).

C. Influence of systematic errors in the database

An important issue for any multipole analysis is the question of how to handle the systematic errors of the experimental results for the different observables used in the database. The ideal database should contain experimental results for both $\gamma p \to p\pi^0$ and $\gamma p \to n\pi^+$, measured simultaneously with one setup for all photon energies and covering the full range of polar angles to minimize energy and angular dependent systematic errors. The analysis of such data would yield a consistent separation of the isospin 1/2 and 3/2 parts from the partial waves of the $p\pi^0$ and $n\pi^+$ reaction channels. However, the isospin separation will fail if there is a considerable inconsistency, such as a normalization error, between the $\gamma p \to n\pi^+$ and $\gamma p \to p\pi^0$ observables ($d\sigma/d\Omega$, Σ, T, . . .). The existing pion photoproduction data, for example, the SAID database, are far from the requirements of the ideal case. Most of the experimental data are taken at one photon energy at a time, the angular distributions are not measured simultaneously for all angles and, more importantly, the consistency between different measurements is less good than their assigned errors would suggest. When combining data from different experiments into one database, one has the difficult task to account properly for the angular and energy dependent systematic errors. A common procedure is to combine the experimental systematic errors in quadrature with the statistical errors or to multiply all data from one set with a systematic scale error (σ_{sys}) by a common factor f while adding $(f-1)^2/\sigma^2_{sys}$ to the χ^2 [40]. The latter method allows for adjustments of an overall scale (angle independent systematic errors), but not for systematic effects in the shape of the angular distributions which is important for the determination of the small $E2$ amplitude. As shown in the following paragraph, it is the shape of the differential cross section and the photon asymmetry near $\theta = 90°$, however, which is sensitive to the $E2$ amplitude. Combining all existing $p\pi^0$ and $n\pi^+$ data in one database regardless of their consistency will result in mean values for the dominant partial waves (M_{1+} and E_{0+}) but meaningless values for the small partial waves (E_{1+} and M_{1-}). Any reliable partial wave analysis for the small amplitudes will require a careful selection of the experimental results used in the database. In practice one has to choose observables that are sensitive to the small amplitude from

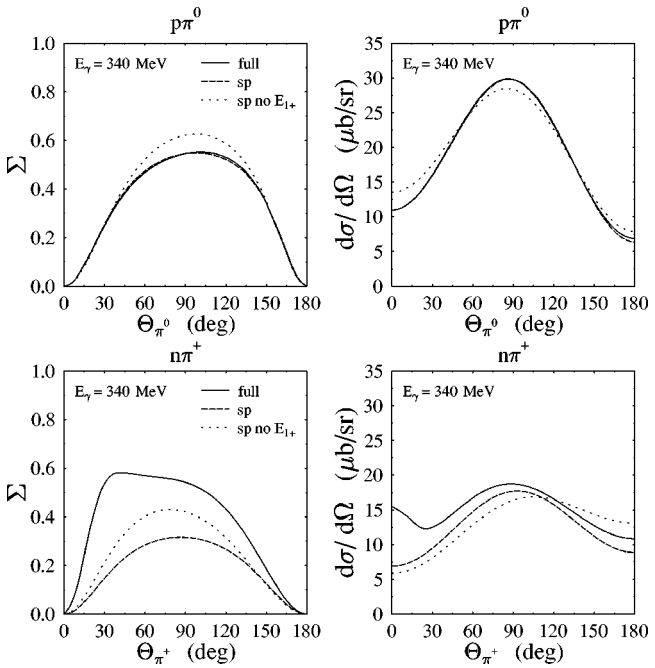

FIG. 10. The sensitivity of differential cross sections $d\sigma/d\Omega$ and photon asymmetries Σ to the E_{1+} multipole and higher partial waves ($l_\pi \geq 2$) for $p(\vec{\gamma},p)\pi^0$ and $p(\vec{\gamma},\pi^+ p)n$ at $E_\gamma = 340$ MeV. The dashed lines are obtained with *s* and *p* waves only. The dotted lines exclude the E_{1+} amplitude and the full lines show the results with all partial waves.

one experiment, or one has to use analyzing methods which are insensitive to energy and angle dependent systematic uncertainties.

Figure 10 shows $d\sigma/d\Omega$ and Σ for different multipole contributions at the $\Delta(1232)$ resonance ($\delta_{33}=90°$). This illustrates the sensitivity to the higher partial waves ($l_\pi \geq 2$) and to the small E_{1+} amplitude. The contribution of the higher partial waves to the $\gamma p \to n\pi^+$ channel is significant at all angles. For the differential cross section at $\theta_{\pi^+}=0°$ and the photon asymmetry around $\theta_{\pi^+}=90°$, the full calculation and the truncation to *s* and *p* waves differ by as much as a factor of 2. The $\gamma p \to p\pi^0$ case is different and one cannot distinguish between the full calculation and the result where only *s* and *p* waves are taken into account. The main reason is that the pion pole term does not contribute in neutral pion photoproduction. Figure 10 shows also the sensitivity of Σ and $d\sigma/d\Omega$ to the small E_{1+} amplitude for both pion channels. The main effects of the E_{1+} multipole in the $p\pi^0$ channel is found near $\theta_{\pi^0}=90°$ for the photon asymmetry and near 0°, 90°, and 180° for the differential cross section. This sensitivity has its origin in the interference term $\mathrm{Re}(E_{1+}M_{1+}^*)$, which appears in the coefficients

$$A \simeq \frac{5}{2}|M_{1+}|^2 - 3\,\mathrm{Re}(E_{1+}M_{1+}^*), \tag{20}$$

$$C \simeq -\frac{3}{2}|M_{1+}|^2 + 9\,\mathrm{Re}(E_{1+}M_{1+}^*), \tag{21}$$

$$A_\Sigma \simeq \frac{3}{2}|M_{1+}|^2 + 3\,\mathrm{Re}(E_{1+}M_{1+}^*), \tag{22}$$

and contributes to both $d\sigma/d\Omega$ and Σ. Without E_{1+} strength the shape of the differential cross section would be determined by $C/A=-3/5$; and the photon asymmetry by $\Sigma(90°)=A_\Sigma/A=3/5$. For $E_{1+}/M_{1+}=-2.5\%$ these values would change to $C/A=-0.7$ and $\Sigma(90°)=0.54$. Setting the E_{1+} multipole to zero (dotted line) results in an increased differential cross section at the extreme angles 0° and 180°, and a lower value at 90°. The photon asymmetry in contrast is enhanced at 90° for $E_{1+}=0$. The same behavior for Σ is found in the $n\pi^+$ channel. In the differential cross section for $n\pi^+$ the effect of E_{1+} is most sizable at the backward angles.

From the above discussion it becomes obvious that a reliable extraction of the small E_{1+} amplitude will require precise photon asymmetry data around 90° and precise data for the differential cross section at all angles.

V. DISCUSSION OF THE DIFFERENT ANALYSES

We have performed three different analyses of our data in order to extract the *s*- and *p*-wave amplitudes, and the $E2/M1$ ratio. First, a fit to the differential cross section and photon asymmetry only in the $\gamma p \to p\pi^0$ channel; second, an energy independent simultaneous multipole analysis of the $\gamma p \to p\pi^0$ and $\gamma p \to n\pi^+$ data to get the isospin separation in the whole energy region (270−420 MeV). In the third analysis an energy dependent fixed-*t* dispersion analysis has been performed, which includes additional observables in order to study the stability of the different multipole solutions.

A. Analysis of the MAMI $p\pi^0$ data

Since the result from the fit to the $\gamma p \to p\pi^0$ channel alone has already been published [11], we summarize here only the key points of our analysis. The $p\pi^0$ angular distributions for the unpolarized cross section $d\sigma_0/d\Omega$, the parallel part $d\sigma_\parallel/d\Omega$ (pion detected in the plane defined by the photon polarization and the photon momentum vector), and perpendicular part $d\sigma_\perp/d\Omega$ can be expressed in the *s*- and *p*-wave approximation by the parametrization

$$\frac{d\sigma_j(\theta)}{d\Omega} = \frac{q}{k}[A_j + B_j\cos(\theta) + C_j\cos^2(\theta)], \tag{23}$$

where q and k denote the center-of-mass momenta of the pion and the photon, respectively, and j indicates the parallel ($\parallel$), perpendicular ($\perp$), and unpolarized (0) components. The coefficients A_j, B_j, and C_j are quadratic or bilinear functions of the *s*- and *p*-wave amplitudes. In particular, $d\sigma_\parallel/d\Omega$ is sensitive to the E_{1^+} amplitude because of interference with M_{1+} in the terms

$$A_\parallel = |E_{0+}|^2 + |3E_{1+} - M_{1+} + M_{1-}|^2, \tag{24}$$

$$B_\parallel = 2\,\mathrm{Re}[E_{0+}(3E_{1+} + M_{1+} - M_{1-})^*], \tag{25}$$

$$C_\parallel = 12\,\mathrm{Re}[E_{1+}(M_{1+} - M_{1-})^*]. \tag{26}$$

Furthermore, the ratio

$$R=\frac{1}{12}\frac{C_{\parallel}}{A_{\parallel}}=\frac{\mathrm{Re}(E_{1+}(M_{1+}-M_{1-})^{*})}{|E_{0+}|^{2}+|3E_{1+}+M_{1+}-M_{1-}|^{2}} \tag{27}$$

is very close to the ratio $R_{EM}=E_{1+}^{3/2}/M_{1+}^{3/2}$ as we will show below. At the $\Delta(1232)$ resonance ($\delta_{33}=90°$) the ratio R can be identified with the R_{EM} value,

$$R\simeq R_{EM}=\left.\frac{\mathrm{Im}\,E_{1+}^{3/2}}{\mathrm{Im}\,M_{1+}^{3/2}}\right|_{W=M_{\Delta}}. \tag{28}$$

This is the key point of our analysis. The method has the advantage of being independent of absolute normalization and insensitive to many systematic errors, because R_{EM} is extracted from the ratio of the coefficients $C_{\parallel}$ and $A_{\parallel}$ fitted to the angular distribution of $d\sigma_{\parallel}/d\Omega$. Analyzing the data by this method the following result is obtained [11]:

$$R_{EM}=-(2.5\pm 0.2_{stat})\%. \tag{29}$$

Without any correction for neglecting the isospin 1/2 contributions to E_{1+} and M_{1+}, the maximum absolute systematic error for R_{EM} would be $\pm 0.5\%$. To further reduce this systematic error one can take the Born contribution and estimate the size of the isospin 1/2 contribution for E_{1+} and M_{1+}. With a conservative estimate the absolute systematic error reduces to less than $\pm 0.2\%$ (see Appendix B for details).

B. Energy independent multipole analysis of the MAMI $p\pi^0$ and $n\pi^+$ data

To obtain the isospin decomposition for the s and p waves in the whole energy range (270−420 MeV), we have performed an energy independent multipole analysis of our data. In this analysis we fit eight parameters, the absolute values of the s and p waves for isospin 1/2 and 3/2 ($E_{0+}^{1/2}$, $E_{0+}^{3/2}$, $M_{1+}^{1/2}$, $M_{1+}^{3/2}$, $E_{1+}^{1/2}$, $E_{1+}^{3/2}$, $M_{1-}^{1/2}$, and $M_{1-}^{3/2}$), to the photon asymmetry and the differential cross section for the $\gamma p\to p\pi^0$ and $\gamma p\to n\pi^+$ reaction channels. Higher partial waves ($l_{\pi}\geqslant 2$) are taken into account by the Born terms, including ρ and ω exchange in the t channel. We obtain the coefficients A, B, and C from the angular distribution of the differential cross section and A_{Σ} from the photon asymmetry. The two-pion reaction channels are described by eight coefficients, which are independent combinations of the isospin 1/2 and 3/2 multipole amplitudes of the s and p waves. In addition, the Fermi-Watson theorem is used to determine the real and imaginary parts of the s- and p-wave multipole amplitudes.

In Fig. 11 we show our fitted multipole amplitudes as $\mathrm{Re}\,\mathcal{M}_{l\pm}^{I}/\cos\delta_{l\pm}^{I}$, which is the absolute value of the amplitude up to a sign that can change with photon energy as in the case of $E_{1+}^{3/2}$. The values of the s- and p-wave amplitudes are fitted independently at each energy to the MAMI data $\gamma p\to p\pi^0$ and $\gamma p\to n\pi^+$. The results for the isospin components for the s- and p-wave amplitudes are presented for 16 photon energy bins [26]. Although systematic errors are greatly reduced because the $p\pi^0$ and $n\pi^+$ data are obtained with the same set up, this method is sensitive to small remaining systematic differences in the results of $d\sigma/d\Omega$ and Σ for the two pion channels, because it relates eight parameters to the eight ''observables'' (A, B, C, and A_{Σ} coefficients for the two-pion channels). Including additional polarization observables in the database and performing an energy dependent multipole analysis overcomes these shortcomings.

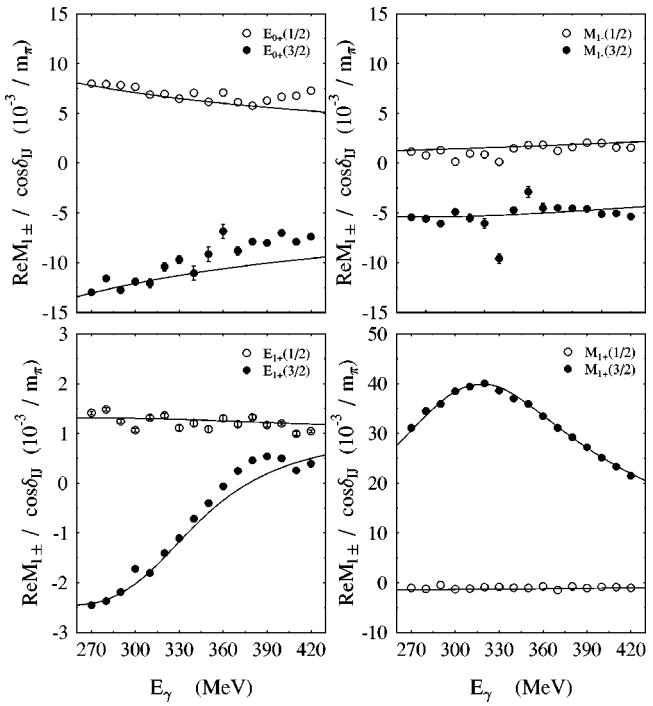

FIG. 11. The isospin $I=1/2$ and $I=3/2$ components of the s- and p-wave multipoles for the proton [26] compared to the energy dependent result of the fixed-t dispersion analysis [27]. The plotted quantities $\mathrm{Re}\,\mathcal{M}_{l\pm}^{I}/\cos\delta_{l\pm}^{I}=\mathcal{M}_{l\pm}^{I}e^{-i\delta_{l\pm}^{I}}$ are equal to the absolute value $|\mathcal{M}_{l\pm}^{I}|$ up to a sign [see Eq. (4)].

C. Energy dependent multipole analysis of the MAMI data

In a third analysis the MAMI pion photoproduction data are analyzed using fixed-t dispersion relations based on Lorentz invariance, isospin symmetry, unitarity, and crossing symmetry [15,27]. This analysis includes the recent MAMI data for the differential cross section $d\sigma/d\Omega$ and photon asymmetry Σ for $p\pi^0$ and $n\pi^+$ from the proton [26,41,42], both older and more recent data from Bonn for the target asymmetry T [43–45], and differential cross section data on π^- production off the neutron from Frascati [46] and recently from TRIUMF [47].

With this method we performed both an energy dependent and an energy independent multipole fit as shown in Fig. 12 by open circles (energy independent) and the solid line (energy dependent). The agreement between the $E_{1^+}^{3/2}$ and $M_{1^+}^{3/2}$ multipole results obtained from the dispersion analysis and the multipole analysis described in the previous section is very good. Both energy independent results show the same energy behavior for the two multipoles. For the real and imaginary parts of the $M_{1^+}^{3/2}$ amplitude the two results are in excellent agreement, the solid dots lying on top of the open circles up to 425 MeV (see Fig. 12). The agreement is also

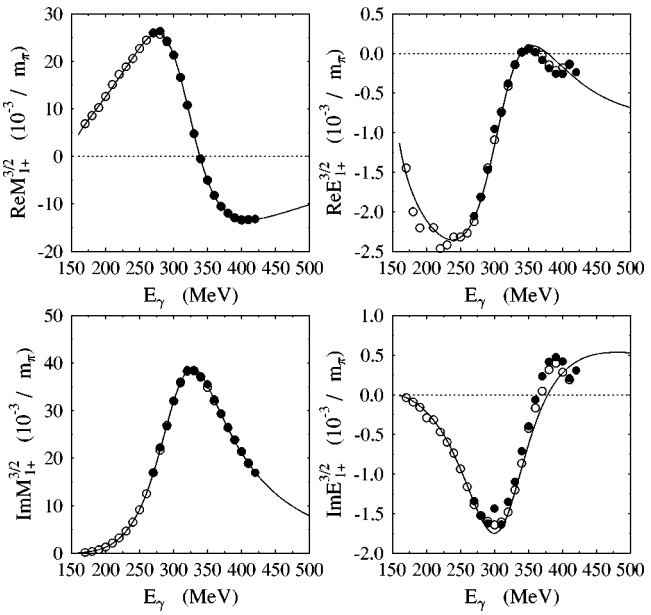

FIG. 12. The real and imaginary isospin $I=3/2$ components of the M_{1+} and E_{1+} multipoles. The solid dots show the result from the energy independent fit only to the MAMI data ($d\sigma/d\Omega$ and Σ) [26]. The solid line and open circles show the energy dependent and energy independent results from the fixed-t dispersion analysis [27].

very good in the case of the small $E_{1+}^{3/2}$ amplitude. In particular, we find that the inclusion of other observables in addition to the MAMI pion photoproduction data decreases the fluctuations slightly for the $E_{1+}^{3/2}$ multipole.

The results of the energy dependent fit (solid line in Fig. 12) agree well with the M_{1+} multipole derived from the energy independent fit, but small systematic differences may be seen for the electric multipole E_{1+} at energies above the $\Delta(1232)$ resonance ($E_\gamma \geqslant 360$ MeV). The ratio R_{EM} at the resonance agrees quite well in both dispersion analyses:

$$R_{EM} = -(2.5 \pm 0.1_{stat})\% \tag{30}$$

for the energy dependent fit and

$$R_{EM} = -(2.33 \pm 0.17_{stat})\% \tag{31}$$

for the energy independent fit.

In addition we have checked the effect of changes in the database. Replacing our differential cross section by the Bonn data obtained in the seventies [48,49] reproduces the results for the leading multipoles but changes the smaller multipoles to some degree (see Table I). The Bonn results for $d\sigma/d\Omega$ at very forward and backward angles force the fit to a smaller E_{1+} value near the resonance. However, it should be kept in mind that the overall compilation of the Bonn $\gamma p \to p\pi^0$ data by Genzel *et al.* [49] results from different experimental setups, which have been reappraised and re-evaluated before combining them into one data set. The main part of the angular distribution ($50° \leqslant \theta_\pi \leqslant 160°$) for $d\sigma/d\Omega$ was measured by detecting the recoil proton in a magnetic spectrometer [50], i.e. by fixed angle and single energy measurements. The differential cross section for $10° \leqslant \theta_\pi \leqslant 70°$ was measured by detecting the two decay photons of the π^0 with lead glass blocks in a different experiment [51]. Each of these experiments has a systematic error of the order of $\pm 5\%$, and it takes much less than this systematic error to change the shape of $d\sigma/d\Omega$ (C/A ratio) and with this the R_{EM} value.

TABLE I. Imaginary parts of the multipoles $E_{1+}^{3/2}$ and $M_{1+}^{3/2}$ in units of $10^{-3}/m_{\pi^+}$, and the ratio $R_{EM} = \mathrm{Im}\, E_{1+}^{3/2}/\mathrm{Im}\, M_{1+}^{3/2}|_{W=M_\Delta}$ in the energy dependent dispersion analysis. The different rows correspond to differential cross section data from MAMI [26,42], LEGS [12], and Bonn [48,49].

Data	$\mathrm{Im}\, M_{1+}^{3/2}$	$\mathrm{Im}\, E_{1+}^{3/2}$	$R_{EM}(\%)$
MAMI	37.66	-0.924	-2.54
LEGS	39.35	-1.276	-3.24
Bonn	38.31	-0.643	-1.68

In the case of the LEGS data the larger cross section leads to larger values for the resonant multipoles $M_{1+}^{3/2}$ and $E_{1+}^{3/2}$. The main reason for this is that the cross section difference between the LEGS and MAMI data is energy dependent (resonance behavior) as shown in Figs. 5 and 6. Inclusion of the polarization data T, Σ, and P from Kharkov [36] does not affect our fit because of the large statistical and systematic errors, especially for the $\gamma p \to p\pi^0$ channel.

VI. DISCUSSION OF THE RESULTS

According to the Fermi-Watson theorem the $E_{1+}^{3/2}$ and $M_{1+}^{3/2}$ partial waves have the same phase δ_{33} and the ratio $E_{1+}^{3/2}/M_{1+}^{3/2}$ is a real quantity. As shown in Fig. 13, this ratio is strongly dependent on the photon energy and varies from -8% at $E_\gamma = 270$ MeV to $+2\%$ at $E_\gamma = 420$ MeV. The ratio R_{EM} is defined at the $\Delta(1232)$ resonance position, where $\delta_{33} = 90°$, by

$$R_{EM} = \left.\frac{E_{1+}^{3/2}}{M_{1+}^{3/2}}\right|_{W=M_\Delta} = \left.\frac{\mathrm{Im}\, E_{1+}^{3/2}}{\mathrm{Im}\, M_{1+}^{3/2}}\right|_{W=M_\Delta}. \tag{32}$$

We note that within the K-matrix fomalism this ratio is free of background contributions since M_Δ is the K-matrix pole. The extraction of the genuine $\Delta(1232)$-resonance parts of the magnetic dipole and electric quadrupole multipoles is model dependent (see for example the work on dynamical models [52–54] and the recently proposed speed plot analysis [15,55]. In order to get a reliable value for R_{EM} it is important to use a database with small angle dependent systematic errors, because the small E_{1+} amplitude depends on the shape of $d\sigma/d\Omega$ and the absolute magnitude of the photon asymmetry at 90°. To obtain a consistent separation for the isospin 1/2 and 3/2 parts of the partial waves, experimental data are required with small inconsistencies in the absolute normalization between the $\gamma p \to p\pi^0$ and $\gamma p \to n\pi^+$ observables. To reduce the influence of such systematics in the multipole analysis, the observables Σ and $d\sigma/d\Omega$ for both reaction channels $p\pi^0$ and $n\pi^+$ were simultaneously measured at all angles and energies with the DAPHNE detector

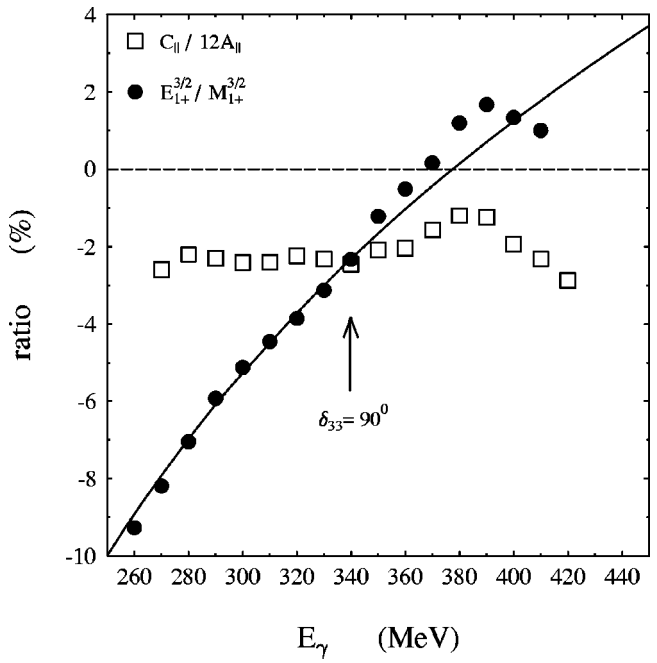

FIG. 13. The energy dependence of the ratio $E_{1+}^{3/2}/M_{1+}^{3/2}$. The solid dots (energy independent) and the solid line (energy dependent) present the result from the fixed-t dispersion multipole analysis [27]. In addition, the energy dependence of $R=C_{||}/(12A_{||})$ is shown as open squares.

at MAMI. The three different analyses to extract R_{EM} from the MAMI data agree very well with each other and, at the $\Delta(1232)$ resonance, we get the final result

$$R_{EM}=\frac{\mathrm{Im}\,E_{1+}^{3/2}}{\mathrm{Im}\,M_{1+}^{3/2}}=-(2.5\pm0.1_{stat}\pm0.2_{sys})\%. \tag{33}$$

In addition, the discussions about the extraction of the correct R_{EM} ratio from our data, which arose in the literature after our first publication [11] can now be summarized as follows. In the Comment of the VPI group [14], our $p\pi^0$ data were included in the SAID database and a value $R_{EM}=-(1.5\pm0.5)\%$ was obtained. As pointed out in our Reply [56], the difference between the VPI result and our value $R_{EM}=-(2.5\pm0.2)\%$ is due to the database used in the SAID analysis. As has been recently confirmed by the VPI group [57], the exclusion of all pre-1980 $p\pi^0$ differential cross section data in the SAID database changes R_{EM} to -2.5%. It is obvious that the key problem arises from the inconsistencies in the different data sets used in the analysis. The forward and backward angles for the differential cross sections used in the SAID database force the VPI solution to smaller R_{EM} values. However, this solution overpredicts the Mainz photon asymmetry data at resonance $\Sigma(90°)=0.58$, compared to the Mainz result $\Sigma(90°)=0.54$. The reason is that at resonance ($\delta_{33}=90°$) the fit has only one parameter, the R_{EM} value, to describe simultaneously the shape of the differential cross section

$$\frac{C}{A}\simeq\frac{-3/2+9R_{EM}}{5/2-3R_{EM}} \tag{34}$$

and the photon asymmetry at 90°

$$\frac{A_\Sigma}{A}\simeq\frac{3/2+3R_{EM}}{5/2-3R_{EM}}. \tag{35}$$

As we have stated before, the compilation of all the existing experimental data into one database can result in mean values for the dominant multipoles and meaningless values for the small multipoles. For example, if one combines the new MAMI data with the Bonn differential cross section results, then the R_{EM} value is affected by small systematic differences in the two data sets. The Bonn differential cross sections range from 10° to 160°, while the MAMI cross sections cover angles from 75° to 125° and are slightly below the Bonn data at $E_\gamma=340$ MeV. In the combined data set the shape of the differential cross section is changed, i.e., the C/A ratio gets smaller. This is the main reason that for the combined Bonn and MAMI data set the R_{EM} value is even below the value which one gets from the Bonn data alone. This influence of the Bonn data on the extracted value of the ratio R_{EM} has been confirmed by the BNL [12] and RPI/VPI groups [58].

In a second Comment [13] our $p\pi^0$ data were analyzed by the RPI group, who obtained the result $R_{EM}=-(3.2\pm0.25)\%$. However, the inclusion of our $n\pi^+$ data in the database lowered this value to $R_{EM}=-(2.64\pm0.25)\%$ [59], in agreement with our analysis.

VII. SUMMARY AND OUTLOOK

We made the first simultaneous and accurate measurements of the differential cross sections and photon asymmetries for the reactions $p(\vec{\gamma},p)\pi^0$ and $p(\vec{\gamma},\pi^+)n$ in the $\Delta(1232)$ region. Using this data we have performed a multipole analysis to obtain the isospin decomposition of the s- and p-wave multipoles and extract the $E2/M1$ ratio over the energy range $270-420$ MeV. Our final results at the $\Delta(1232)$ resonance position ($\delta_{33}=90°$) are $R_{EM}=-(2.5\pm0.1_{stat}\pm0.2_{sys})\%$, and $A_{1/2}=-(131\pm1)(10^{-3}/\sqrt{\mathrm{GeV}})$ and $A_{3/2}=-(251\pm1)(10^{-3}/\sqrt{\mathrm{GeV}})$ for the helicity amplitudes.

In the meantime, more $p(\vec{\gamma},\pi^0)p$ data [60] for the differential cross section and the photon asymmetry have been taken. This new experiment covers the full range of polar angles by observing the two decay photons in the TAPS detector at MAMI. The analysis is in progress and will produce new differential cross sections for the extreme forward and backward angles. In this way we hope also to clarify the absolute normalization problem in the differential cross section between LEGS and MAMI.

ACKNOWLEDGMENTS

The authors wish to acknowledge the excellent support of K. H. Kaiser and H. Euteneuer, and the accelerator group of MAMI, as well as many other scientists and technicians of the Institut für Kernphysik at Mainz, DAPNIA/SPhN at

Saclay and INFN at Pavia. We would also like to thank H. Arenhövel, H. Schmieden, and P. Wilhelm for fruitful discussions and comments. This work was supported by the Deutsche Forschungsgemeinschaft (SFB 201) and the U.K. Engineering and Physical Sciences Research Council.

APPENDIX A

The coefficients A, B, C, and A_Σ in the s- and p-wave approximation for the differential cross section and the photon asymmetry:

$$A(s_{wave},p_{wave})=|E_{0+}|^2+\frac{9}{2}|E_{1+}|^2+\frac{5}{2}|M_{1+}|^2 -|M_{1-}|^2-3\,\mathrm{Re}(E_{1+}(M_{1+}-M_{1-})^*) +\mathrm{Re}(M_{1-}M_{1+}^*),$$

$$B(s_{wave},p_{wave})=2\,\mathrm{Re}(E_{0+}(3E_{1+}+M_{1+}-M_{1-})^*),$$

$$C(s_{wave},p_{wave})=\frac{9}{2}|E_{1+}|^2-\frac{3}{2}|M_{1+}|^2 +9\,\mathrm{Re}(E_{1+}(M_{1+}-M_{1-})^*) -3\,\mathrm{Re}(M_{1-}M_{1+}^*),$$

$$A_\Sigma(s_{wave},p_{wave})=-\frac{9}{2}|E_{1+}|^2+\frac{3}{2}|M_{1+}|^2 +3\,\mathrm{Re}(E_{1+}(M_{1+}-M_{1-})^*) +3\,\mathrm{Re}(M_{1-}M_{1+}^*).$$

The differential cross section up to $l_\pi=2$ partial waves

$$\frac{d\sigma}{d\Omega}=\frac{q}{k}[A+B\cos(\theta)+C\cos^2(\theta)+D\cos^3(\theta)+E\cos^4(\theta)]$$

has five coefficients with

$$A=A(s_{wave},p_{wave})+\frac{5}{2}|E_{2-}|^2+\frac{45}{4}|E_{2+}|^2 +\frac{9}{2}|M_{2-}|^2+\frac{9}{2}|M_{2+}|^2 +\mathrm{Re}(E_{0+}(-6E_{2+}-3M_{2+}-E_{2-}+3M_{2-})^*) +\mathrm{Re}\left(E_{2-}\left(\frac{15}{2}E_{2+}+3M_{2-}+3M_{2+}\right)^*\right) +\mathrm{Re}\left(M_{2-}\left(-9M_{2+}-\frac{9}{2}E_{2+}\right)^*\right)+\mathrm{Re}\left(\frac{9}{2}M_{2+}E_{2+}^*\right),$$

$$B=B(s_{wave},p_{wave}) +2\,\mathrm{Re}(M_{1+}(E_{2-}-9E_{2+}+9M_{2+}+6M_{2-})^*) +\mathrm{Re}(M_{1-}(18E_{2+}-2E_{2-}+9M_{2+}+6M_{2-})^*) +6\,\mathrm{Re}(E_{1+}(-2E_{2-}+3M_{2-}+3M_{2+}+3E_{2+})^*),$$

$$C=C(s_{wave},p_{wave})-\frac{3}{2}|E_{2-}|^2+\frac{27}{2}|E_{2+}|^2+\frac{9}{2}|M_{2-}|^2 +27|M_{2+}|^2+\mathrm{Re}(E_{0+}(6E_{2+}+3M_{2+}+E_{2-}-3M_{2-})^*) +\mathrm{Re}(E_{2-}(-63E_{2+}-9M_{2-}+9M_{2+})^*) +\mathrm{Re}(M_{2-}(81E_{2+}+81M_{2+})^*)-\mathrm{Re}(81M_{2+}E_{2+}^*),$$

$$D=2\,\mathrm{Re}(M_{1+}(30E_{2+}-12M_{2+}-18M_{2-})^*) +\mathrm{Re}(M_{1-}(-30E_{2+}-15M_{2+})^*) +\mathrm{Re}(E_{1+}(-36M_{2-}+36M_{2+}+18E_{2+}+18E_{2-})^*),$$

$$E=\frac{45}{4}|E_{2+}|^2-\frac{45}{2}|M_{2+}|^2-90\,\mathrm{Re}(M_{2+}M_{2-}^*) +\frac{45}{2}\mathrm{Re}(E_{2+}(5M_{2+}-5M_{2-}+3E_{2-})^*).$$

The photon asymmetry Σ

$$\Sigma\frac{d\sigma}{d\Omega}\frac{1}{\sin^2\theta}=\frac{q}{k}(A_\Sigma+B_\Sigma\cos\theta+C_\Sigma\cos^2\theta)$$

has three coefficients with

$$A_\Sigma=A_\Sigma(s_{wave},p_{wave})-\frac{3}{2}|E_{2-}|^2-9|E_{2+}|^2-\frac{9}{2}|M_{2-}|^2 +\mathrm{Re}(E_{0+}(E_{2-}+E_{2+}+M_{2-})^*) +\mathrm{Re}\left(E_{2-}\left(3M_{2-}+\frac{21}{2}E_{2+}\right)^*\right)-\frac{9}{2}\mathrm{Re}(E_{2+}M_{2-}^*),$$

$$B_\Sigma=+3\,\mathrm{Re}(M_{1+}(5E_{2+}+4M_{2+}+6M_{2-})^*) -3\,\mathrm{Re}(M_{1-}(5E_{2+}-5M_{2+})^*) -3\,\mathrm{Re}(E_{1+}(9E_{2+}-9E_{2-})^*),$$

$$C_\Sigma=\frac{45}{2}|M_{2+}|^2-45|E_{2+}|^2 +\frac{45}{2}\mathrm{Re}(E_{2+}(3E_{2-}-2M_{2-}-M_{2+})^*) +90\,\mathrm{Re}(M_{2+}3M_{2-}^*).$$

APPENDIX B

At the $\Delta(1232)$ resonance position, where the phase δ_{33} passes through 90° ($E_\gamma\simeq 340$ MeV) we find $\mathrm{Re}\,M_{1^+}(3/2)=0$, $\mathrm{Re}(M_{1^+}-M_{1^-})\simeq 0$, and negligible contributions from higher partial waves ($l_\pi\geqslant 2$) (see Sec. IV B). The ratio R of the coefficients $A_{||}$ and $C_{||}$ for $p(\vec{\gamma},p)\pi^0$ can then be expressed by

$$R=\frac{C_\parallel}{12A_\parallel}=\frac{\mathrm{Re}(E_{1+}(M_{1+}-M_{1-})^*)}{|E_{0+}|^2+|3E_{1+}-M_{1+}+M_{1-}|^2}.$$

Neglecting $|E_{0+}|^2$, $9|E_{1+}|^2$, and all terms with $\mathrm{Re}(M_{1+}-M_{1-})$ results in

$$R=\frac{\mathrm{Im}\,E_{1+}\mathrm{Im}(M_{1+}-M_{1-})}{-6\,\mathrm{Im}\,E_{1+}\mathrm{Im}(M_{1+}-M_{1-})+\mathrm{Im}^2(M_{1+}-M_{1-})}.$$

Dividing by $\mathrm{Im}^2(M_{1+}-M_{1-})$ we obtain

$$R=\frac{R_{\pi^0}}{1-6R_{\pi^0}},$$

with

$$R_{\pi^0}=\frac{\mathrm{Im}\,E_{1+}}{\mathrm{Im}\,M_{1+}-\mathrm{Im}\,M_{1-}}.$$

If we further neglect $\mathrm{Im}\,M_{1-}$ and the isospin 1/2 components $\mathrm{Im}\,M_{1+}^{1/2}$ and $\mathrm{Im}\,E_{1+}^{1/2}$, then the largest correction comes from $\mathrm{Im}\,E_{1+}^{1/2}$, which is of the order of $10-20\,\%$ of $\mathrm{Im}\,E_{1+}$. The final result depends on the ratio of $\mathrm{Im}\,E_{1+}^{1/2}/\mathrm{Im}\,E_{1+}(p\pi^0)$. If we further assume $R=-2.5\%$ we obtain

(a) For $\mathrm{Im}\,E_{1+}^{1/2}=0$,

$$R=\frac{C_\parallel}{12A_\parallel}\simeq\frac{1.R_{EM}}{1-6.R_{EM}}\rightarrow R_{EM}=-2.95\%;$$

(b) For $\mathrm{Im}\,E_{1+}^{1/2}/\mathrm{Im}\,E_{1+}=10\%$,

$$R=\frac{C_\parallel}{12A_\parallel}\simeq\frac{1.1R_{EM}}{1-6.6R_{EM}}\rightarrow R_{EM}=-2.65\%;$$

(c) For $\mathrm{Im}\,E_{1+}^{1/2}/\mathrm{Im}\,E_{1+}=20\%$,

$$R=\frac{C_\parallel}{12A_\parallel}\simeq\frac{1.2R_{EM}}{1-7.2R_{EM}}\rightarrow R_{EM}=-2.45\%,$$

with

$$R_{EM}=\frac{\mathrm{Im}\,E_{1+}^{3/2}}{\mathrm{Im}\,M_{1+}^{3/2}}.$$

Without any correction for the isospin 1/2 contributions to E_{1+} and M_{1+} the maximum systematic error of R_{EM} would be $\pm 0.5\%$ absolute. To further reduce this systematic error we can estimate the size of the isospin 1/2 contribution by the Born contribution. A conservative estimate of the remaining systematic error is less than $\pm 0.2\%$ absolute.

[1] A. Rujula, H. Georgi, and S. L. Glashow, Phys. Rev. D **12**, 147 (1975).
[2] C. Becchi and G. Morpurgo, Phys. Lett. **17**, 352 (1965).
[3] R. Koniuk and N. Isgur, Phys. Rev. D **21**, 1868 (1980).
[4] S. S. Gershteyn *et al.*, Yad. Fiz. **34**, 1566 (1981) [Sov. J. Nucl. Phys. **34**, 870 (1981)].
[5] D. Drechsel and M. M. Giannini, Phys. Lett. **143B**, 329 (1984).
[6] S. Capstick, Phys. Rev. D **46**, 2864 (1992).
[7] A. Wirzba and W. Weise, Phys. Lett. B **188**, 6 (1987).
[8] K. Bermuth *et al.*, Phys. Rev. D **37**, 89 (1988).
[9] D. B. Leinweber, Proceedings of the International Conference Baryons92, 1992, p. 29.
[10] A. Buchmann *et al.*, Phys. Rev. C **55**, 448 (1997).
[11] R. Beck and H.-P. Krahn *et al.*, Phys. Rev. Lett. **78**, 606 (1997).
[12] G. S. Blanpied *et al.*, Phys. Rev. Lett. **79**, 4337 (1997).
[13] R. M. Davidson and N. C. Mukhopadhyay, Phys. Rev. Lett. **79**, 4509 (1997).
[14] G. Keaton and R. L. Workman, Phys. Rev. Lett. **79**, 4511 (1997).
[15] O. Hanstein *et al.*, Phys. Lett. B **385**, 45 (1996).
[16] R. Crawford *et al.*, Nucl. Phys. **A603**, 303 (1996).
[17] D. Lohmann and J. Peise *et al.*, Nucl. Instrum. Methods Phys. Res. A **343**, 494 (1994).
[18] A. Schmidt, Diplomarbeit, University Mainz, 1995.
[19] H. Herminghaus, K. H. Kaiser, and H. Euteneuer, Nucl. Instrum. Methods Phys. Res. **138**, 1 (1976).
[20] I. Anthony *et al.*, Nucl. Instrum. Methods Phys. Res. A **301**, 230 (1991).
[21] S. Hall *et al.*, Nucl. Instrum. Methods Phys. Res. A **368**, 698 (1996).
[22] F. Rambo *et al.*, Phys. Rev. C **58**, 489 (1998).
[23] A. Kraus *et al.*, Phys. Rev. Lett. **79**, 3834 (1997).
[24] G. Audit *et al.*, Nucl. Instrum. Methods Phys. Res. A **301**, 473 (1991).
[25] A. Braghieri *et al.*, Nucl. Instrum. Methods Phys. Res. A **343**, 623 (1994).
[26] H.-P. Krahn, Dr. thesis, University Mainz, 1996.
[27] O. Hanstein, D. Drechsel, and L. Tiator, Nucl. Phys. **A632**, 561 (1998).
[28] M. Jacob and G. C. Wick, Ann. Phys. (N.Y.) **7**, 404 (1959).
[29] G. F. Chew, M. I. Goldberger, F. E. Low, and V. Nambu, Phys. Rev. **106**, 1345 (1957).
[30] A. S. Raskin and T. W. Donnelly, Ann. Phys. (N.Y.) **191**, 78 (1989).
[31] D. Drechsel and L. Tiator, J. Phys. G **18**, 449 (1992).
[32] I. Barker *et al.*, Nucl. Phys. **B95**, 347 (1975).
[33] W. Chiang and F. Tabakin, Phys. Rev. C **55**, 2054 (1997).
[34] R. Workman, Phys. Rev. C **53**, 1434 (1996).
[35] V. Grushin, in *Photoproduction of Pions on Nucleons and Nuclei*, Proceedings of the Lebedev Physics Institute Academy of Science of the USSR (Nova Science Publishers, New York and Budapest, 1989), Vol. 186.
[36] V. A. Get'man *et al.*, Nucl. Phys. **B188**, 397 (1981); A. Belyaev *et al.*, *ibid.* **B213**, 201 (1983).
[37] K. M. Watson, Phys. Rev. **182**, 228 (1954).
[38] A. Donnachie, Rep. Prog. Phys. **36**, 695 (1973).
[39] R. Arndt, I. Strakovsky, and R. Workman, Phys. Rev. C **53**, 430 (1996).

[40] G. D'Agostini, Nucl. Instrum. Methods Phys. Res. A **346**, 306 (1994). The same method is used in the LEGS analysis.
[41] M. Fuchs *et al.*, Phys. Lett. B **368**, 20 (1996).
[42] F. Härter, Dr. thesis, University Mainz, 1996.
[43] H. Dutz *et al.*, Nucl. Phys. **A601**, 319 (1996).
[44] D. Menze *et al.*, Compilation of pion photoproduction data, Bonn, 1977.
[45] K. Buechler *et al.*, Nucl. Phys. **A570**, 580 (1994).
[46] F. Carbonara *et al.*, Nuovo Cimento A **13**, 59 (1973).
[47] A. Bagheri *et al.*, Phys. Rev. C **38**, 875 (1988).
[48] G. Fischer *et al.*, Z. Phys. **253**, 38 (1972).
[49] H. Genzel *et al.*, Z. Phys. **268**, 43 (1974).
[50] G. Fischer *et al.*, Z. Phys. **245**, 225 (1971).
[51] E. Hilger *et al.*, Z. Phys. **268**, 19 (1974).
[52] A. M. Bernstein *et al.*, Phys. Rev. C **47**, 1274 (1993).
[53] T. Sato and T.-S. Lee, Phys. Rev. C **54**, 2660 (1996).
[54] P. Wilhelm *et al.*, Phys. Rev. C **54**, 1423 (1996).
[55] Th. Wilbois *et al.*, Phys. Rev. C **57**, 295 (1998).
[56] R. Beck and H.-P. Krahn, Phys. Rev. Lett. **79**, 4512 (1997).
[57] R. L. Workman, nucl-th/9810013.
[58] R. M. Davidson *et al.*, Phys. Rev. C **59**, 1059 (1999).
[59] R. M. Davidson, private communication.
[60] R. Leukel, Dr. thesis, University Mainz, 1999.
[61] A. M. Sandorfi, Few-Body Syst., Suppl. **99**, 1 (1998).